Heavy Doping and Band Engineering by Potassium to Improve the Thermoelectric Figure of Merit in p-Type PbTe, PbSe, and PbTe[subscript 1– y]Se[subscript y]

Citation: Zhang, Qian, Feng Cao, Weishu Liu, Kevin Lukas, Bo Yu, Shuo Chen, Cyril Opeil, David Broido, Gang Chen, and Zhifeng Ren. " Heavy Doping and Band Engineering by Potassium to Improve the Thermoelectric Figure of Merit in p-Type PbTe, PbSe, and PbTe[subscript 1– y]Se[subscript y]." Journal of the American Chemical Society 134, no. 24 (June 20, 2012): 10031–10038.

As Published: http://dx.doi.org/10.1021/ja301245b

Publisher: American Chemical Society

Persistent URL: http://hdl.handle.net/1721.1/86875

Version: Author's final manuscript: final author's manuscript post peer review, without publisher's formatting or copy editing

Heavy doping and band engineering by potassium to improve thermoelectric figure-of-merit in p-type PbTe, PbSe, and $PbTe_{1-y}Se_y$

Qian Zhang,[†] Feng Cao,[†] Weishu Liu,[†] Kevin Lukas,[†] Bo Yu,[†] Shuo Chen,[†] Cyril Opeil,[†] David Broido,[†] Gang Chen,*[‡] and Zhifeng Ren**[†]

[†] Department of Physics, Boston College, Chestnut Hill, Massachusetts 02467, USA

[‡] Department of Mechanical Engineering, Massachusetts Institute of Technology, Cambridge, Massachusetts 02139, USA

ABSTRACT:

We present detailed studies of potassium (K) doping in $PbTe_{1-y}Se_y$ (y = 0, 0.15, 0.25, 0.75, 0.85, 0.95, and 1). It was found that Se increases the doping concentration of K in PbTe due to the balance of electronegativity and also lowers the lattice thermal conductivity because of the increased point defects. By tuning the composition and carrier concentration to increase the density of states around the Fermi level, higher Seebeck coefficients are obtained from the two valence bands of $PbTe_{1-y}Se_y$. A peak thermoelectric figure-of-merit (ZT) of ~1.6 is obtained in Te-rich $K_{0.02}Pb_{0.98}Te_{0.75}Se_{0.25}$ at 773 K and of ~1.7 in Se-rich $K_{0.02}Pb_{0.98}Te_{0.15}Se_{0.85}$ at 873 K. However, the average ZT is higher in Te-rich compositions with the best found in $K_{0.02}Pb_{0.98}Te_{0.75}Se_{0.25}$ than the Se-rich compositions, such a result is due to the improved electron transport by heavy K doping with the assistance of Se.

INTRODUCTION

Intensive attention has recently been paid to energy conversion using thermoelectric principles, which can directly convert both waste heat and solar energy into electricity.[1-3] Large scale applications call for thermoelectric materials with high dimensionless figure-of-merit $ZT = [S^2\sigma/(\kappa_{L+}\kappa_e)]T$, where S is the Seebeck coefficient, σ the electrical conductivity, κ_L the lattice thermal conductivity, κ_e the charge carrier thermal conductivity, and T the absolute temperature.[4-7] Accordingly, a combination of high Seebeck coefficient with high electrical conductivity and low thermal conductivity is desired and has been pursued. However, it is difficult to optimize one parameter without deteriorating the others. Complex crystals are normally considered to have the advantage of decoupling the inter-related three quantities with the concept of "electron–crystal phonon–glass".[8-10] Nanostructuring is the major approach for *ZT* enhancement since it allows independent tuning of all the parameters.[11-17]

Lead telluride (PbTe) with simple face-centered cubic rock salt structure is one of the most studied thermoelectric materials suitable for the intermediate temperature range (600-800 K).[18-21] Its cheaper sister compound, lead selenide (PbSe), has also decent *ZT*.[22-24] Excellent progress has recently been made through band engineering, such as resonant states [18-19, 23] and bands convergence,[20, 22, 25-26] leading to improvements in both the electrical conductivity and Seebeck coefficient simultaneously without too much affecting the thermal conductivity.[27] Good results were reported in Tl doped PbTe, which pushed *ZT* value to ~1.5 at 773 K by creating resonant states near the Fermi energy.[18] Recently, Al doping was reported to have resulted in n-type resonant doping in PbSe with a peak *ZT* of ~1.3.[23] A great deal of theoretical work has been performed to find possible new resonant dopants in PbTe and PbSe.[28-30] It was predicted that alkali metals (K-, Rb-, and Cs-) can create resonant density of states (DOSs) distortion in PbTe, but not Na since Na does not change the DOS near the top of the valence band.[28] However, PbTe doped heavily with Na still led to high *ZT* values, which is believed to be the result of the coexistence of light (*L*) - and heavy (Σ) - valence bands in PbTe.[31] Effective doping of Na moves the Fermi level close to the Σ band, which has much larger DOS, helping increase the Seebeck coefficient.[20, 32-34] A *ZT* value of

~1.4 at 750 K in Na doped PbTe with a Hall carrier concentration p_H > ~7.5×10^{19} cm^{-3} is obtained.[20] A similar effect has been shown theoretically and experimentally in PbSe, which has a flat, high mass, high DOS band roughly 0.35-0.4 eV below the valence band maximum.[35] The *ZT* value reaches ~1.2-1.3 at 850 K for Na doped PbSe with a Hall carrier concentration between 9×10^{19} and 1.5×10^{20} cm^{-3}.[22] Furthermore, by alloying with Se, *ZT* of ~1.8 at ~850 K was reported for $Na_{0.02}Pb_{0.98}Te_{0.85}Se_{0.15}$.[25] Regardless of whether the increase in electronic power factor is due to resonant levels or the Σ band, it is obvious that band engineering can enhance the carrier (electrons/holes) transport. Indeed, both resonant states and band convergence benefit the high *ZT* in Tl doped PbTe.[26] However, it is desired to avoid Tl for practical applications due to its toxicity. Motivated by recent calculations,[28] we chose to study K doping to make $K_xPb_{1-x}Te_{1-y}Se_y$, because of the smaller ionic radius of K^+ compared with Rb^+ and Cs^+. Normally, it is believed that K has a limited soluability in PbTe,[26, 36] which limits the Hall carrier concentration to less than 6×10^{19} cm^{-3}. So very limited report was on K doping in PbTe, in contrast to Na doping in PbTe that can produce much higher carrier concentration. In this paper, we are able to increase the Hall carrier concentration to ~(8-15)$\times10^{19}$ cm^{-3} in PbTe by K doping with the help of Se through the balance of electronegativity. It is shown that band engineering works well in $K_xPb_{1-x}Te_{1-y}Se_y$, giving higher Seebeck coefficient. Peak *ZT* values of ~1.6 and ~1.7 are obtained in Te-rich $K_{0.02}Pb_{0.98}Te_{0.75}Se_{0.25}$ and Se-rich $K_{0.02}Pb_{0.98}Te_{0.15}Se_{0.85}$, respectively. However the average *ZT* of the Te-rich compositions is higher, and so more favorable for practical applications.

EXPERIMENTAL SECTION

Synthesis, Ingots with nominal compositions $K_xPb_{1-x}Te$ (x = 0.01, 0.0125, 0.015, and 0.02), $K_xPb_{1-x}Se$ (x = 0, 0.005, 0.01, 0.0125, and 0.025), and $K_{0.02}Pb_{0.98}Te_{1-y}Se_y$ (y = 0.15, 0.25, 0.75, 0.85, and 0.95, other compositions such as y = 0.4 and 0.5 were also studied but the results not shown here to increase the readability of the figures) were prepared in a quartz tube with carbon coating. The raw materials inside the quartz tube were slowly raised to 1000-1100 ^oC and kept for 6 h, then slowly cooled to 650 ^oC and stayed at that temperature for 50 h, finally slowly cooled to room temperature. The obtained ingots were cleaned and hand milled in a glove box. The sieved (325 mesh) powder was loaded into the half-inch die and hot pressed at

500-600 ^{o}C for 2 min. The hot pressed pellets were sealed in quartz tube for further annealing at 600 ^{o}C for 4 h to make the sample stable during the measurements at temperatures up to 600 ^{o}C.

Characterizations, X-ray diffraction spectra analysis was conducted on a PANalytical multipurpose diffractometer with an X'celerator detector (PANalytical X'Pert Pro). The electrical resistivity (ρ) was measured by a four-point dc current-switching method together with the Seebeck coefficient based on the static temperature difference method, both of which were conducted on a commercial system (ULVAC ZEM-3). The thermal diffusivity (α) was measured on a laser flash apparatus (Netzsch LFA 447) and the specific heat (C_p) was measured on a differential scanning calorimetry thermal analyzer (Netzsch DSC200-F3). The volumetric density (D) was measured by the Archimedes method and shown in Table 1 compared with the theoretical density D_T. The thermal conductivity κ was calculated using $\kappa = D\alpha C_p$. The Hall Coefficient R_H at room temperature was measured using the PPMS (Physical Properties Measurement System, Quantum Design). The Hall carrier concentration n_H and Hall mobility μ_H were calculated using $n_H = 1/(eR_H)$ and $\mu_H = \sigma R_H$. It is understood that there is a 3% error on electrical conductivity, 5% on Seebeck coefficient, and 4% on thermal conductivity, so it is 10% for power factor and 11% for ZT value. For better readability of the figures, we deliberately plot the curves without the error bars.

Table 1. Theoretical density D_T, measured volumetric density D, relative density D_R and power law exponents, δ, of electrical conductivity for $K_xPb_{1-x}Te$, $K_xPb_{1-x}Se$, and $K_{0.02}Pb_{0.98}Te_{1-y}Se_y$.

	$K_xPb_{1-x}Te$				$K_xPb_{1-x}Se$			$K_{0.02}Pb_{0.98}Te_{1-y}Se_y$				
x/y	0.01	0.0125	0.015	0.02	0.01	0.0125	0.015	0.15	0.25	0.75	0.85	0.95
D_T (gcm^{-3})	8.18	8.18	8.17	8.14	8.19	8.18	8.18	8.09	8.10	8.13	8.13	8.14
D (gcm^{-3})	8.06	8.02	8.02	8.01	7.84	7.9	7.92	7.97	7.99	7.97	7.91	8.02
D_R	99%	98%	98%	98%	96%	97%	97%	99%	99%	98%	97%	99%
δ	3.11	2.95	3	2.94	3.17	2.8	2.99	2.34	2.4	2.58	2.9	2.87

RESULTS AND DISCUSSION

Comparing the ionic radius of Pb, Na, and K, shown in Table 2, K^+ is closer to Pb^{2+}, but a little bigger.

Table 2 Ionic radius and Pauling's electronegativity of K, Na, Pb, Te, and Se

	K	**Na**	**Pb**	**Te**	**Se**
Ionic radius (Å)	1.33	0.97	1.20	2.11	1.91
Pauling's electronegativity	0.82	0.93	2.33	2.10	2.55

For samples $K_xPb_{1-x}Te$ (x = 0.01, 0.0125, 0.015, and 0.02), the electrical conductivity, Seebeck coefficient, power factor, thermal diffusivity, specific heat, lattice thermal conductivity, and total thermal conductivity were measured and presented in Figure 1(a)-(f), respectively. The electrical conductivity at room temperature increases a little bit with increasing K concentration, but no change is seen at high temperature, where all samples show a decrease with temperature (Fig. 1(a)). The Seebeck coefficients of all samples, shown in Fig. 1(b), change only slightly, which is likely due to the contributions from both the light and heavy holes with the high carrier concentration.[26] Power factor increases with increasing K concentration and peaks at about 500 K, shown in Fig. 1(c). The diffusivity of all samples is basically the same, shown in Fig. 1(d), consistent with the microstructures, see Supporting Information. The specific heat of all samples, shown in Fig. 1(e), is similar indicating good repeatability of the measurements. Combining the diffusivity, specific heat, and volumetric density, gives the thermal conductivities (Fig. 1(f)), which are very close to each other.

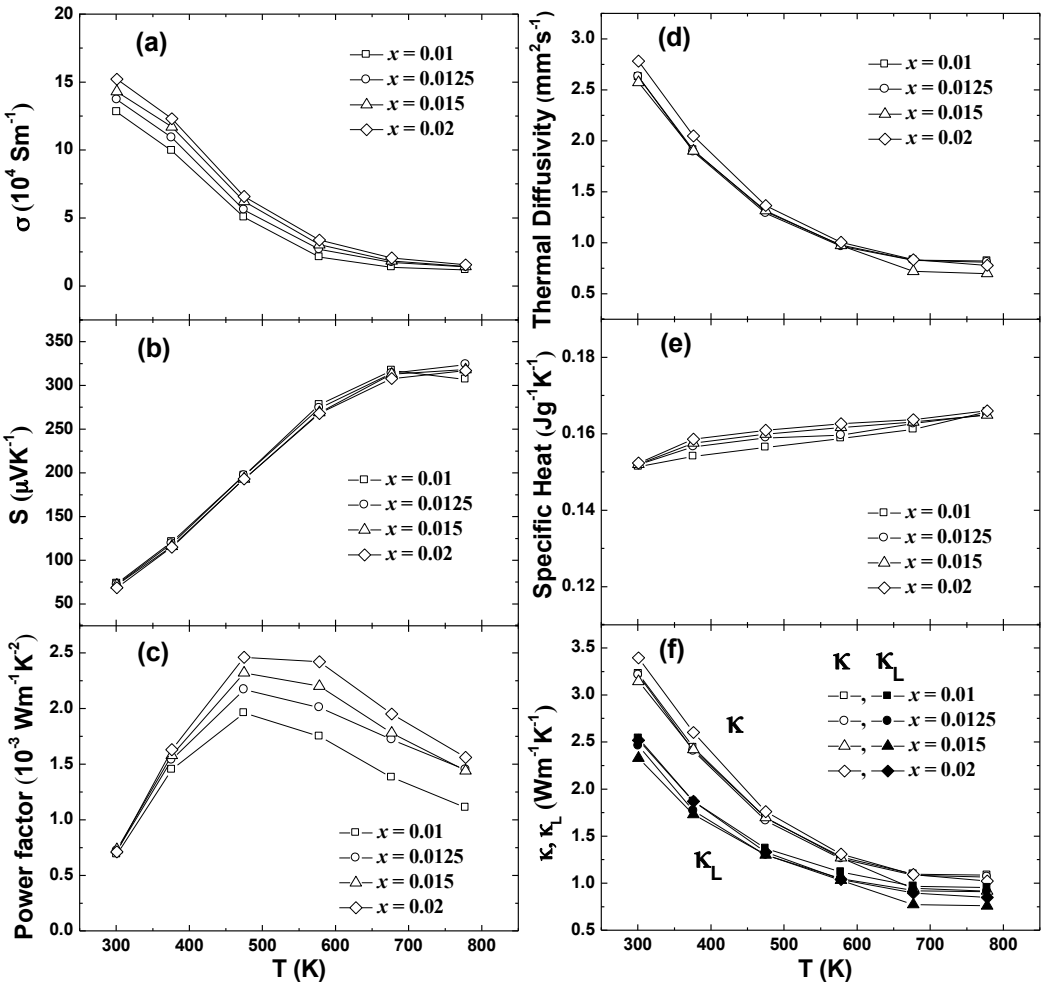

Figure 1. Temperature dependence of electrical conductivity (a), Seebeck coefficient (b), power factor (c), thermal diffusivity (d), specific heat (e), total thermal conductivity and lattice thermal conductivity (f) for $K_xPb_{1-x}Te$ (x = 0.01, 0.0125, 0.015, and 0.02).

To better understand the band structure of $K_xPb_{1-x}Te$, the room temperature Seebeck coefficient as a function of Hall carrier concentration is plotted in Fig. 2 (filled circles). Compared with the reported results (open circles and half open circles).[20, 32] The Hall carrier concentration of our K doped PbTe samples ($< 6.3\times10^{19}$ cm^{-3}) is lower than Na doped PbTe, which could be as high as 14×10^{19} cm^{-3}. The flattening of the Seebeck coefficient with increasing carrier concentration indicates a contribution from the second valence band. This behavior has been explained previously using a multiband model with a Kane model describing the nonparabolic light hole band (L band) and a parabolic heavy hole band (Σ band) [25, 26, 37], and we employ a similar model here.

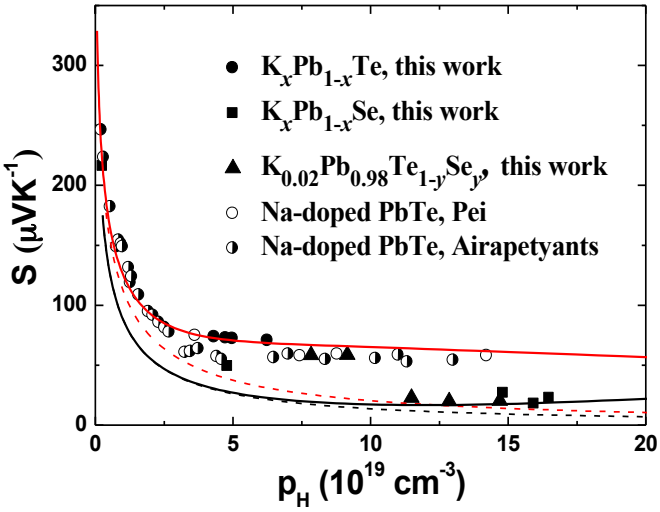

Figure 2. Room temperature Pisarenko plots for $K_xPb_{1-x}Te$ (x = 0.01, 0.0125, 0.015, and 0.02, filled circles), $K_xPb_{1-x}Se$ (x = 0, 0.005, 0.010, 0.0125, and 0.015, filled squares), and $K_{0.02}Pb_{0.98}Te_{1-y}Se_y$ (y = 0.15, 0.25, 0.75, 0.85, and 0.95, filled triangles) in comparison with reported data on Na-doped PbTe by Pei *et al.*[20] (open circles) and Airapetyants *et al.*[32] (half open circles). Dashed black curve is based on single nonparabolic band model with the light hole effective mass of PbSe m^*/m_e = 0.28. Solid black curve is based on two bands model (light nonparabolic band and heavy parabolic band) with the heavy hole effective mass of PbSe m^*/m_e = 2.5. Dashed red curve is based on single nonparabolic band model with the light hole effective mass of PbTe m^*/m_e = 0.36. Solid red curve is based on two bands model (light nonparabolic band and heavy parabolic band) with the heavy hole effective mass of PbTe m^*/m_e = 2.

The Seebeck coefficient, S_L, and carrier concentration, p_L, for a single non-parabolic light hole band at the L point is

$$S_L = \pm \frac{k_B}{e}\left[\frac{{}^1F_{-2}^1(\eta,\alpha)}{{}^0F_{-2}^1(\eta,\alpha)} - \eta\right] \quad (1)$$

$$p_L = \frac{1}{3\pi^2}\left(\frac{2m_L^* k_B T}{h^2}\right)^{3/2} {}^0F_0^{3/2}(\eta,\alpha) \quad (2)$$

where k_B is the Boltzmann constant, e the electron charge, ${}^nF_k^m$ is the generalized Fermi function[37], η is the reduced Fermi level, h is Planck's constant, and m_L^* is the light hole density of states effective mass, taken as $m_L^*/m_e = 0.36$[37]. The non-parabolicity parameter, α

= k_BT/E_g, where E_g is the L-point band gap, and we have assumed that deformation potential scattering by acoustic phonons dominates [20, 25, 37]. We have also done the calculation including ionized impurity scattering for the nonparabolic light hole band. The relaxation time for inoized impurities, τ_I, is much larger than that for deformation potential scattering, τ_D. Combining the relaxation times using Matheiessen's rule: $1/\tau=1/\tau_I+ 1/\tau_D$, there is almost no difference in the light hole Seebeck coefficient from the results when only the τ_D was included. For the heavy hole band, taken along the Σ direction in Brillouin zone[37], the Seebeck coefficient, S_Σ, and carrier concentration, p_Σ are,

$$S_\Sigma = \frac{k_B}{e}\left[\frac{{}^1F^1_{-2}(\eta_\Sigma,0)}{{}^0F^1_{-2}(\eta_\Sigma,0)} - \eta_\Sigma\right] \tag{3}$$

$$p_\Sigma = \frac{1}{3\pi^2}\left(\frac{2m^*_\Sigma k_B T}{h^2}\right)^{3/2} {}^0F^{3/2}_0(\eta_\Sigma,0) \tag{4}$$

Here, m^*/m_e = 2[38] is the density of states effective mass for the heavy holes, $\eta_\Sigma = \eta - \Delta E/k_BT$, where ΔE is the energy difference between the light-hole and heavy hole band maxima whose value is discussed below. Note that for this parabolic band, α = 0. The total Seebeck coefficient from both hole bands, S_{total}, is taken to be:

$$S_{total} = \left(\sigma_L S_L + \sigma_\Sigma S_\Sigma\right)/\left(\sigma_L + \sigma_\Sigma\right) \tag{5}$$

where σ_L and σ_Σ are the electrical conductivity from L and Σ bands, respectively.[37]

The total Hall carrier concentration for a two-band system, p_H, is related to the carrier concentrations in each band, p_L and p_Σ, as described previously in Refs. 25 and 37. This expression is provided in the Supplementary information and Refs 25 and 37. In Fig. 2, the solid red line shows the calculated S_{total} vs. p_H for PbTe. It can be seen that the data (filled circles) falls nicely on the flat part of the solid red line at S ~75 μVK^{-1}, indicating a clear contribution from two bands by K doping. Alternatively, Kanatzidis *et al.* obtained the flat at S ~56 μVK^{-1} using the light hole effective mass ~0.2m_e, which can explain Na doped PbTe pretty well.[26] The magnitude of the heavy hole contribution can be highlighted by examining a one-band light hole model obtained by removing the heavy hole band contribution. This case gives the dashed red line shown in Fig. 2, which falls well below the measured data for high carrier concentration.

When temperature increases, the Seebeck coefficient increases dramatically to ~320 μVK^{-1} at 775 K, even much higher than that in Na doped PbTe ~260 μVK^{-1} at 775 K believed due to two bands contribution.[20] Considering the prediction of possible resonant states introduced by K doping through first principles calculation[28], it is likely that resonant doping may also play a minor role here in addition to two bands contribution. However, we do not have enough evidence to support this because the Seebeck is not high enough. The limited carrier concentration < 6×10^{19} cm^{-3} by K doping restrains the increase of the electrical conductivity (shown in Fig. 1 (a)), which is the determining factor for the *S* flattening. Furthermore, the decrease of electrical conductivity with temperature is faster in K doped samples, exhibited by the power law exponents, δ, of the electrical conductivity ($\sigma \approx T^{-\delta}$) presented in Table 1.

Generally speaking, the total thermal conductivity κ is the sum of the charge carrier thermal conductivity κ_e and the lattice thermal conductivity κ_L, where κ_e can be calculated via the Wiedemann-Franz relation, $\kappa_e = L\sigma T$, with the Lorenz number L the same for the electrons and holes, κ_L is then derived by subtracting κ_e from κ and presented in Figure 1(f). Again, multiband model is employed for the accurate estimation of L, which gives[37]:

$$L_L = \left(\frac{k_B}{e}\right)^2 \left\{ \frac{{}^2F_{-2}^1(\eta,\alpha)}{{}^0F_{-2}^1(\eta,\alpha)} - \left[\frac{{}^1F_{-2}^1(\eta,\alpha)}{{}^0F_{-2}^1(\eta,\alpha)}\right]^2 \right\} \tag{6}$$

$$L_\Sigma = \left(\frac{k_B}{e}\right)^2 \left\{ \frac{{}^2F_{-2}^1(\eta_\Sigma,0)}{{}^0F_{-2}^1(\eta_\Sigma,0)} - \frac{{}^1F_{-2}^1(\eta_\Sigma,0)}{{}^0F_{-2}^1(\eta_\Sigma,0)} \right\} \tag{7}$$

$$L_{total} = \left(\sigma_L L_L + \sigma_\Sigma L_\Sigma\right)/\left(\sigma_L + \sigma_\Sigma\right) \tag{8}$$

Where L_L, L_Σ and L_{total} are the Lorenz numbers from L band, Σ band and both bands, respectively. Because of the low electrical conductivity, the carrier thermal conductivity is also low. With almost the same lattice thermal conductivity (the same lattice scattering), we achieved lower total thermal conductivity compared with Na-doped PbTe.[20] The highest *ZT* value is ~1.3 at ~673 K for $K_{0.015}Pb_{0.985}Te$ shown in Figure 3, which is comparable with Na doped PbTe at the same temperature.[20]

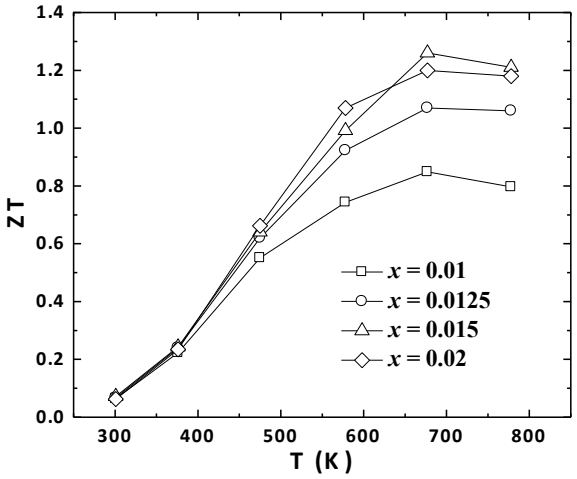

Figure 3. Temperature dependence of *ZT* for $K_xPb_{1-x}Te$ (x = 0.01, 0.0125, 0.015, and 0.02).

In both Pb-Te and Pb-Se systems, K^+ and Na^+ dopants substitute Pb^{2+}, and both K and Na substitutions reduce the Pauling's electronegativity (PE) of Pb^{2+}, shown in Table 2. In spite of the comparable ionic radius, the solubility of K and Na is determined by the difference of electronegativity between the average anions (Te^{2-} or Se^{2-}) and cations (Pb^{2+} together with K^+ or Na^+) after doping. Typically, larger difference results in higher solubility. Since K has a lower electronegativity than Na, the average cation electronegativity after doping will always be lower in the case of K substitution. For Pb-Te, lower average cation electronegativity reduces the electronegativity difference between Te^{2-} and Pb^{2+}, so K has less solubility than Na in Pb-Te. For Pb-Se, the situation is opposite (lower average cation electronegativity enlarges the electronegativity difference between Se^{2-} and Pb^{2+}), thus K has higher solubility than Na in Pb-Se.

With different K concentrations, samples $K_xPb_{1-x}Se$ (x = 0, 0.005, 0.010, 0.0125, and 0.015) were prepared and measured. The electrical conductivity, Seebeck coefficient, power factor, thermal diffusivity, specific heat, and thermal conductivity are shown in Figures. 4(a)-(f), respectively. It is clear that when $x \geq 0.01$, the electrical conductivity increases dramatically. The room temperature Hall carrier concentration is increased to $\sim 1.6\times10^{20}$ cm^{-3} (shown in Fig. 2, filled squares). Again we draw the room temperature Pisarenko plots for single nonparabolic band model (dashed black line) and multi-band model (solid black line). Here we have taken with the effective mass of light hole $m_L^*/m_e = 0.28$[23] and heavy hole $m_\Sigma^*/m_e = 2.5$ for PbSe, which was obtained from a first principles calculation[39], There is not

much difference between the two models, suggesting that most of the contribution comes from the light hole band at room temperature, which agrees well with the previous results.[22] The pinning of the Fermi level by the heavy band happens only at the high temperature when the offset value of the two bands is small enough. High Seebeck coefficient ~210 μVK^{-1} at 875 K can be obtained with the contribution from both bands. Since band gap of PbSe increases with temperature (~0.43 eV at 850 K vs. ~0.28 eV at 300 K), the Seebeck coefficient goes up all the way with increasing temperature without any sign of the bipolar effect. The low lattice thermal conductivity, ~1.7 at 300 K and ~0.6 $Wm^{-1}K^{-1}$ at high temperature, similar with the previously reported values[22], is calculated here for K-doped PbSe with *L* obtained from Eqs. 6, 7 and 8. We noticed that the electrical conductivity decreases rapidly with increasing temperature, indicated by δ shown in Table 1. However, with the high start point of the electrical conductivity and the high Seebeck coefficient, the maximum *ZT* value reached was ~1.2 at 873 K, as shown in Figure 5, but the average *ZT* is clearly lower than that of K doped $K_xPb_{1-x}Te$. Both the maximum *ZT* and the average *ZT* are comparable with Na doped PbSe.

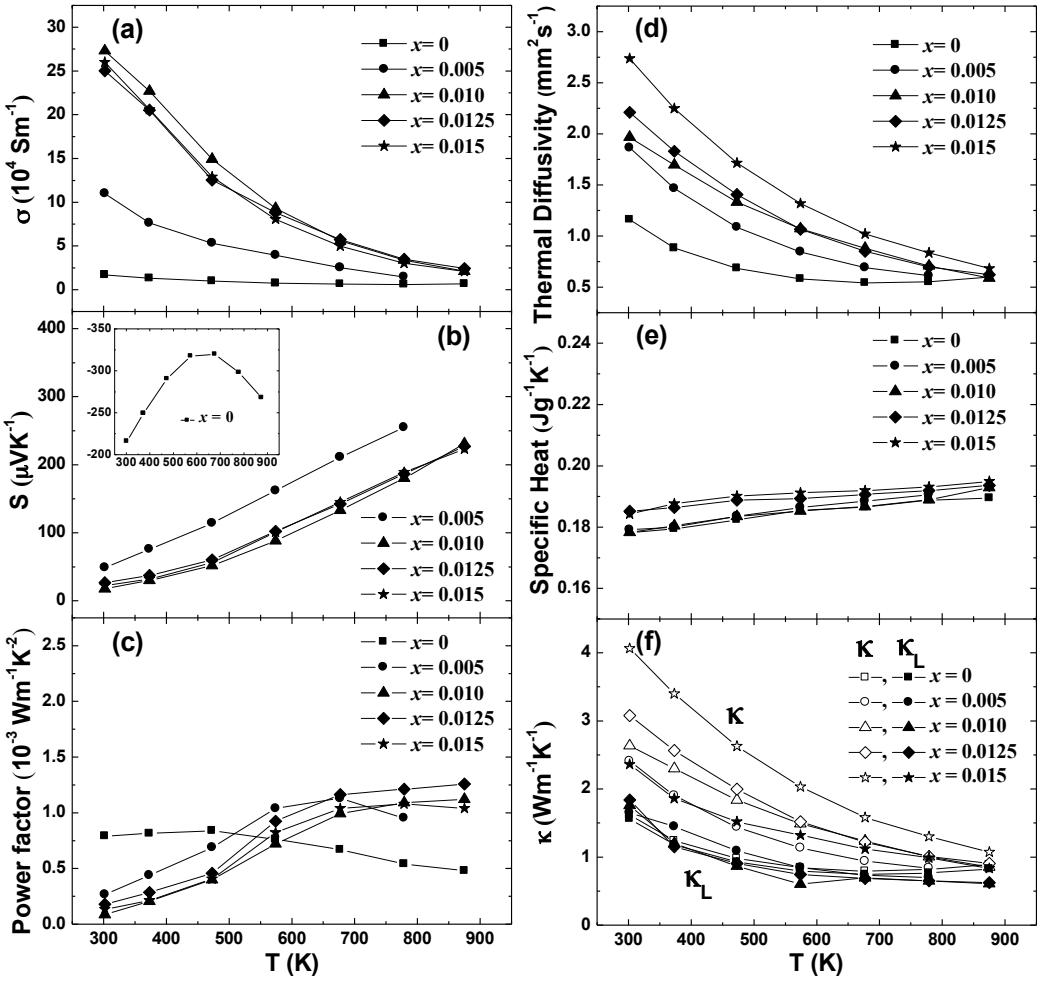

Figure 4. Temperature dependence of electrical conductivity (a), Seebeck coefficient (b), power factor (c), thermal diffusivity (d), specific heat (e), total thermal conductivity and lattice thermal conductivity (f) for $K_xPb_{1-x}Se$ (x = 0, 0.005, 0.010, 0.0125, and 0.015).

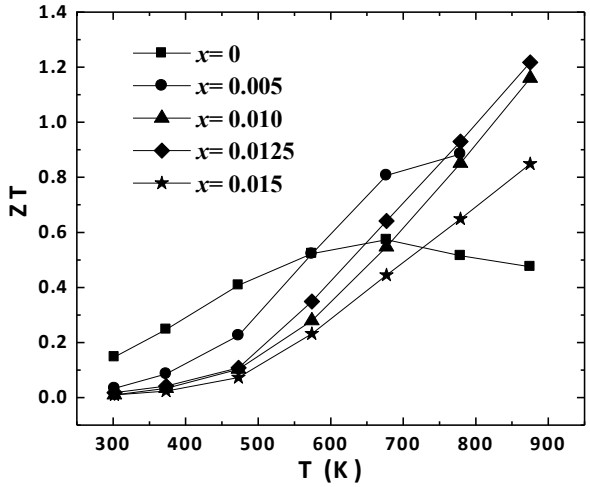

Figure 5. Temperature dependence of ZT for $K_xPb_{1-x}Se$ (x = 0, 0.005, 0.010, 0.0125, and 0.015).

After studying the K doping in PbTe and PbSe independently, we turned our attention to studying K doping in $PbTe_{1-y}Se_y$ aiming at simultaneously increasing the power factor and further reducing the thermal conductivity to achieve higher *ZT*. We fixed the K concentration at 2% in the Pb site based on the results of K in PbTe and PbSe, with different Se concentrations presented: $K_{0.02}Pb_{0.98}Te_{1-y}Se_y$ (y = 0.15, 0.25, 0.75, 0.85, and 0.95). All the X-Ray diffraction spectra (Figure 6) show single phase with face-centered cubic rock salt structure. The peaks shift right with increasing concentration of Se because of the smaller lattice parameters. Good solid solution is confirmed by good fitting to the Vegard' law (inset of Figure 6).

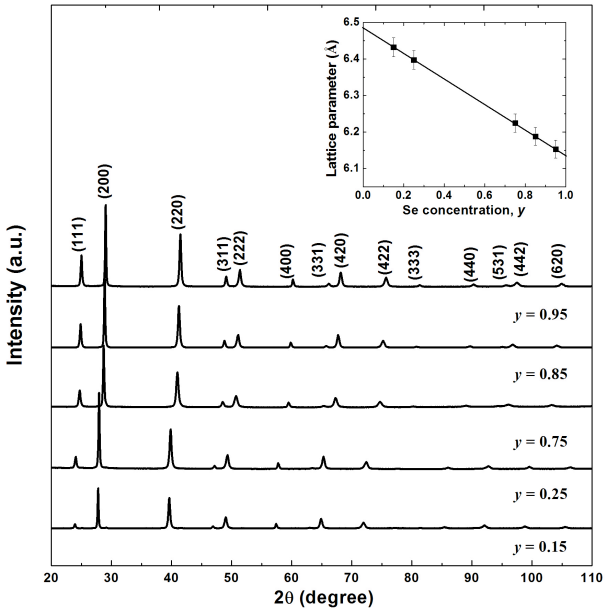

Figure 6. XRD patterns of $K_{0.02}Pb_{0.98}Te_{1-y}Se_y$ (y = 0.15, 0.25, 0.75, 0.85, and 0.95). The inset shows the lattice parameter relation with the Se concentration in $K_{0.02}Pb_{0.98}Te_{1-y}Se_y$.

Figure 7 shows the room temperature Hall carrier concentration as a function of K concentration (a) and Se concentration (b). With the help of Se, the Hall carrier concentration is increased effectively from $< 6\times10^{19}$ cm^{-3} in PbTe to the optimized concentration of $(8\text{-}15)\times10^{19}$ cm^{-3} for $PbTe_{1-y}Se_y$, consistent with the observed values in the previous reports.[20, 22] Together with the room temperature Seebeck coefficient, the Pisarenko plot of the solid solution samples is shown in Figure 2 (filled triangles). Noticeable deviation of the Seebeck coefficient from the single band model (dashed red line) for $K_{0.02}Pb_{0.98}Te_{1-y}Se_y$ (y = 0.15 and

0.25) supports the effects of heavy hole bands. Owing to the relative small effective mass and larger energy difference between heavy hole and light hole band edges, ΔE, in PbSe, the Seebeck coefficients are lower than those of K doped PbTe (filled circles). For $K_{0.02}Pb_{0.98}Te_{1-y}Se_y$ (y = 0.75, 0.85, and 0.95), more features come from K doped PbSe. As temperature increases, two bands start to converge. We find good fits to the data using the energy differences between conduction (C) band edge and L and Σ hole band edges:

$$\begin{aligned} \Delta E_{C-L} &= 0.18 + (4T/10000) - 0.04y \\ \Delta E_{C-\Sigma} &= 0.42 + 0.10y \end{aligned} \tag{9}$$

where y is the concentration of Se.[37, 40] It has been concluded that the convergence of the electronic bands can provide more benefit for the enhancement of Seebeck coefficient from double bands.[25] However, L band will move gradually below Σ band at certain temperature and depart from the convergence when y = 0 (PbTe). So we use Se to increase the T_{cvg}, which gives the most optimized Seebeck coefficient at high temperature, demonstrated in Figure 8 (b). With increase of Se, the temperature for highest Seebeck coefficient increases. The highest Seebeck coefficient is ~320 μVK^{-1} at 775 K, much higher than that in Na doped $PbTe_{1-y}Se_y$ ~220 μVK^{-1} at 775 K. The successfully improved carrier concentration compensates the loss in the carrier mobility for the increased scattering of the electrons, which keeps the electrical conductivity the same at low temperature, see Figure 8(a). Fortunately, the decrease of the electrical conductivity is slowed down with temperature, giving a smaller δ shown in Table 1. As a result, the power factor is enhanced at high temperature as shown in Figure 8(c).

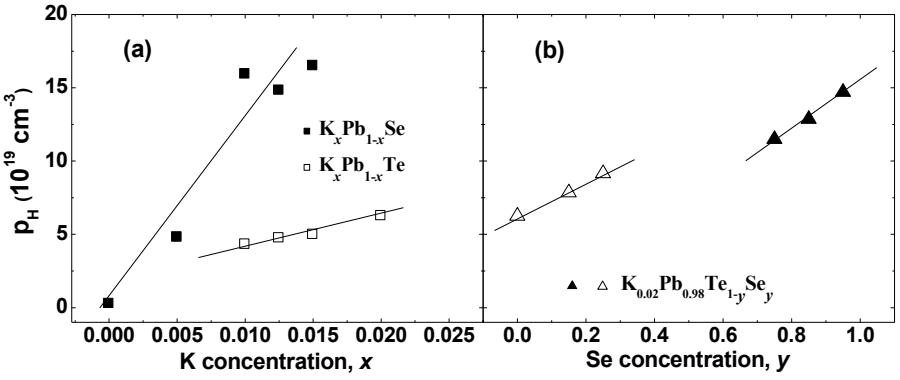

Figure 7. Hall carrier concentration at room temperature as a function of K concentration (a) and Se concentration (b).

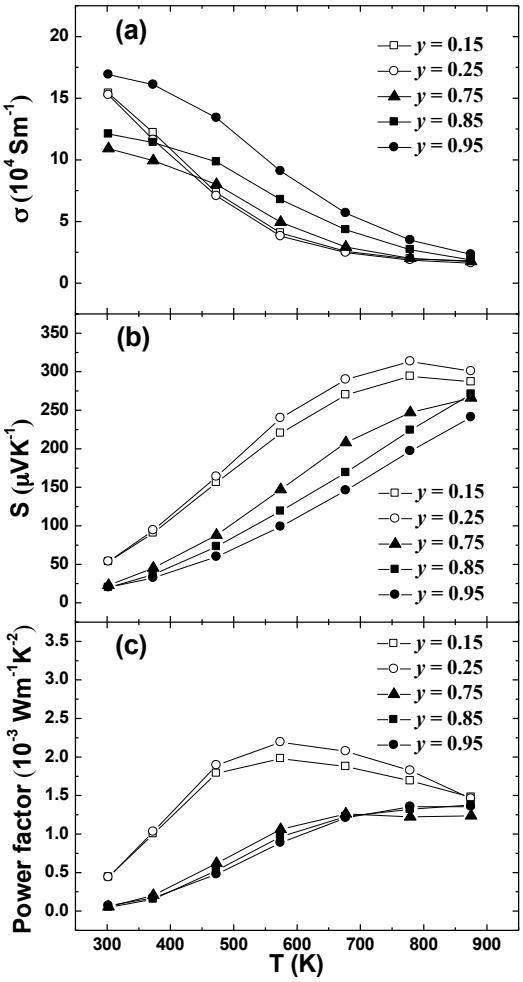

Figure 8. Temperature dependence of electrical conductivity (a), Seebeck coefficient (b) and power factor (c) for $K_{0.02}Pb_{0.98}Te_{1-y}Se_y$ (y = 0.15, 0.25, 0.75, 0.85, and 0.95).

The other obvious but very important role Se plays is to decrease the lattice thermal conductivity by alloying scattering when it is used together with Te. The thermal diffusivity, specific heat, total thermal conductivity, and lattice thermal conductivity for $K_{0.02}Pb_{0.98}Te_{1-y}Se_y$ (y = 0.15, 0.25, 0.75, 0.85, and 0.95) are shown in Figure 9(a)-(c), respectively. The increased lattice thermal conductivity at 800 K in figure 9 (c) may come from the error of calculated L. It seems that more Se ($K_{0.02}Pb_{0.98}Te_{0.15}Se_{0.85}$) can increase the peak ZT to ~1.7 at ~873 K in comparison with ~1.6 in $K_{0.02}Pb_{0.98}Te_{0.75}Se_{0.25}$ at ~773 K (Figure 10), but clearly Te-rich composition is more promising for any applications below 873 K since the average ZTs are much higher.

Up to now, only Tl has been shown to induce the resonant states in p-type PbTe with

extraordinary increase in Seebeck coefficient.[18] However, with the help of a second valence band in PbTe, high *ZT* can also be obtained by heavy doping with Na, K and Mg, especially when combining the alloy scattering introduced by PbSe or PbS.[20, 25, 26, 41, 42] Additionally, typical nanostructures have been created in PbTe matrix to lower the lattice thermal conductivity by adding a second phase and ball milling.[43, 44] Other group IIIA elements (Al, Ga and In)[45-47], VIIA elements[21] and some rare-earth elements[48] are proved good n-type dopants. A *ZT* >1.5 at 775 K is reached in La doped PbTe with Ag_2Te nanoscale precipitates.[48] With decent *ZT*s in both p-type and n-type, PbTe is a promising candidate for TE applications in the near future.

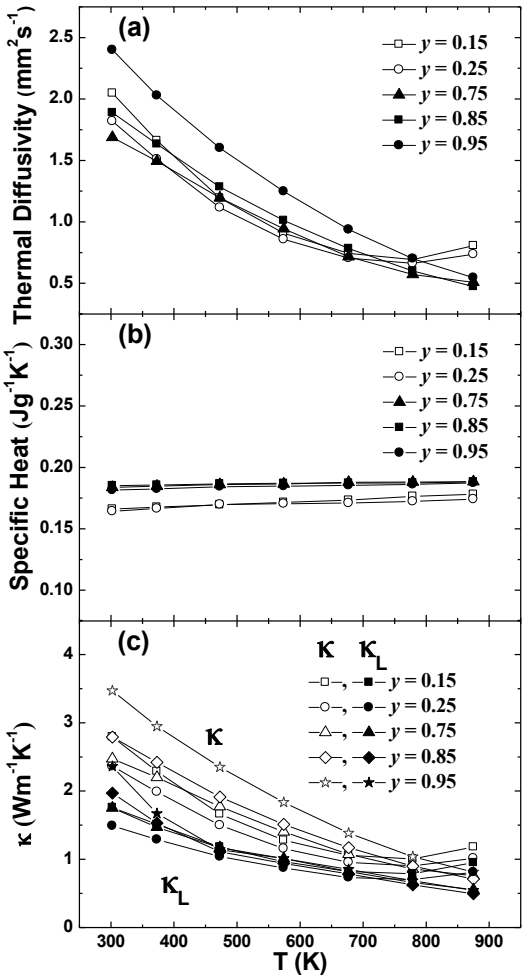

Figure 9. Temperature dependence of thermal diffusivity (a), specific heat (b), total thermal conductivity and lattice thermal conductivity (c) for $K_{0.02}Pb_{0.98}Te_{1-y}Se_y$ (y = 0.15, 0.25, 0.75, 0.85, and 0.95).

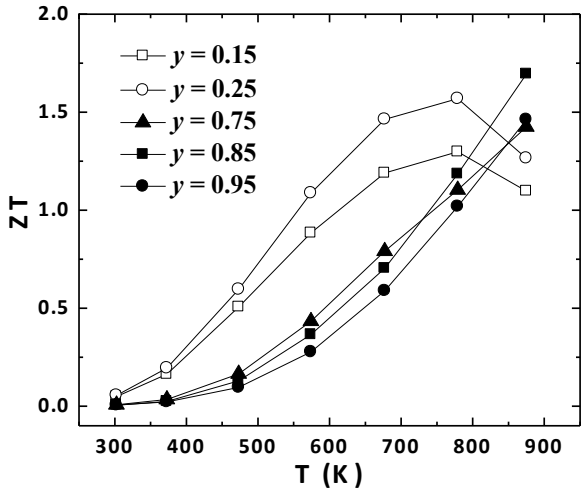

Figure 10. Temperature dependence of *ZT* for $K_{0.02}Pb_{0.98}Te_{1-y}Se_y$ (y = 0.15, 0.25, 0.75, 0.85, and 0.95).

CONCLUDING REMARKS

Potassium, an acceptor dopant in $K_xPb_{1-x}Te_{1-y}Se_y$, can strongly enhance the Seebeck coefficient by activating the heavy hole band via heavy doping, which increases DOS near the Fermi level. Combined with a lower lattice thermal conductivity due to increased point defects and the increased electrical conductivity at high temperature, higher peak *ZT* values of ~1.6 were obtained in Te-rich samples $K_{0.02}Pb_{0.98}Te_{0.75}Se_{0.25}$ at 773 K and ~1.7 in Se-rich samples $K_{0.02}Pb_{0.98}Te_{0.15}Se_{0.85}$ at 873 K, but the average *ZT* of the Te-rich samples is much higher than those of the Se-rich samples even though Te is more expensive, so a trade-off between cost and performance needs to be considered for practical applications.

AUTHOR INFORMATION

Corresponding Author

*gchen2@mit.edu

**renzh@bc.edu

ACKNOWLEDGEMENT: This work is supported by "Solid State Solar-Thermal Energy Conversion Center (S^3TEC)", an Energy Frontier Research Center founded by the U.S. Department of Energy, Office of Science, Office of Basic Energy Science under award number DE-SC0001299 (G. C. and Z. F. R.).

SUPPORTING INFORMATION AVAILABLE

The microstructures and chemical composition for some samples; Room temperature Pisarenko plots for $K_xPb_{1-x}Te$ (x = 0.01, 0.0125, 0.015, and 0.02), $K_xPb_{1-x}Se$ (x = 0, 0.005, 0.010, 0.0125, and 0.015), and $K_{0.02}Pb_{0.98}Te_{1-y}Se_y$ (y = 0.15, 0.25, 0.75, 0.85, and 0.95) using $\Delta E_{C-\Sigma} = 0.36$ eV; This information is available free of charge via the Internet at http://pubs.acs.org/

REFERENCES

(1) Rowe, D. M. *CRC Handbook of Thermoelectrics*; CRC Press, Boca Raton, 1995.

(2) Disalvo, F. J. *Science* **1999**, *285*, 703.

(3) Kraemer, D.; Poudel, B.; Feng, H. P.; Cavlor, J. C.; Yu, B.; Yan, X.; Ma, Y.; Wang, X. W.; Wang, D. Z.; Muto, A.; McEnaney, K.; Chiesa, M.; Ren, Z. F.; Chen, G. *Nature Materials* **2011**, *10*, 532.

(4) Harman, T. C.; Taylar, P. J.; Walsh, M. P.; LaForge, B. E. *Science* **2002**, *297*, 2229.

(5) Yan, X.; Joshi, G.; Liu, W. S.; Lan, Y. C.; Wang, H.; Lee, S.; Simonson, J. M.; Poon, S. J.; Tritt, T. M.; Chen, G.; Ren, Z. F. *Nano Lett*. **2011**, *11*, 556.

(6) Zhang, Q.; He, J.; Zhu, T. J.; Zhang, S. N.; Zhao, X. B.; Tritt, T. M. *Appl. Phys. Lett.* **2008**, *93*, 102109.

(7) Poudel, B.; Hao, Q.; Ma, Y.; Lan, Y. C.; Minnich, A.; Yu, B.; Yan, X.; Wang, D. Z.; Muto, A.; Vashaee, D.; Chen, X.; Liu, J.; Dresselhaus, D. S.; Chen, G.; Ren, Z. F. *Science*, **2008**, *320*, 634.

(8) Sales, B. C.; Mandrus, D.; Williams, R. K. *Science*, **1996**, *272*, 1325.

(9) Yu, C.; Zhu, T. J.; Zhang, S. N.; Zhao, X. B.; He, J.; Su, Z.; Tritt, T. M. *J. Appl. Phys.* **2008**, *104*, 013705.

(10) Kleinke, H. *Chem. Mater.* **2010**, *22*, 604.

(11) Dresselhaus, M. S.; Chen, G.; Tang, M. Y.; Yang, R. G.; Lee, H.; Wang, D. Z.; Ren, Z. F.; Fleurial, J. P.; Gogna, P. *Adv. Mater.* **2007**, *19*, 1043.

(12) Liu, W. S.; Yan, X.; Chen, G.; Ren, Z. F. *Nano Energy* **2012**, *1*, 42.

(13) Martin, J.; Wang, L.; Chen, L. D.; Nolas, G. S. *Phys. Rev. B* **2009**, *79*, 115311.

(14) Faleev, S. V.; Leonard, F. *Phys. Rev. B* **2008**, *77*, 214304.

(15) Zhang, Q.; Zhang, Q. Y.; Chen, S.; Liu, W. S.; Lukas, K.; Yan, X.; Wang, H. Z.; Wang, D. Z.; Opeil, C.; Chen, G.; Ren, Z. F. *Nano Energy* **2012**, *1*, 183.

(16) Scheele, M.; Oeschler, N.; Meier, K.; Kornowski, A.; linke, C.; Weller, H. *Adv. Funct. Mater.* **2009**, *19*, 1.

(17) Zhang, Q., Sun, T.; Cao, F.; Li, M.; Hong, M. H.; Yuan, J. K.; Yan, Q. Y.; Hng, H. H.; Wu, N. Q.; Liu, X. G. *Nanoscale* **2010**, *2*, 1256.

(18) Heremans, J. P.; Jovovic, V.; Toberer, E. S.; Samarat, A.; Kurosaki, K.; Charoenphakdee, A.; Yamanaka, S.; Snyder, G. J. *Science* **2008**, *321*, 554.

(19) Yu, B.; Zhang, Q. Y.; Wang, H.; Wang, X. W.; Wang, H. Z.; Wang, D. Z.; Snyder, G. J.; Chen, G.; Ren, Z. F. *J. Appl. Phys.* **2010**, *108*, 016104.

(20) Pei, Y.; LaLonde, A.; Iwanaga, S.; Snyder, G. J. *Energy Environ. Sci.* **2011**, *4*, 2085.

(21) LaLonde, A. D.; Pei, Y. Z.; Snyder, G. J. *Energy Environ. Sci.* **2011**, *4*, 2090.

(22) Wang, H.; Pei, Y.; LaLonde, A. D.; Snyder, G. J. *Adv. Mater.* **2011**, *23*, 1366.

(23) Zhang, Q. Y.; Wang, H.; Liu, W. S.; Wang, H. Z.; Yu, B.; Zhang, Q.; Tian, Z. T.; Ni, G.; Lee, S.; Esfarjani, K.; Chen, G.; Ren, Z. F. *Energy Environ. Sci.* **2012**, *5*, 5246.

(24) Androulakis, J.; lee, Y.; Todorov, I.; Chung, D. Y.; Kanatzidis, M. *Phys. Rev. B* **2011**, *83*, 195209.

(25) Pei, Y.; Shi, X.; LaLonde, A.; Wang, H.; Chen, L.; Snyder, G. J. *Nature* **2011**, *473*, 66.

(26) Androulakis, J.; Todorov, I.; Chung, D. Y.; Ballikaya, S.; Wang, G.; Uher, C.; Kanatzidis, M. *Phys. Rev. B* **2010**, *82*, 115209.

(27) Delaire, O.; Ma, J.; Marty, K.; May, A. F.; McGuire, M. A.; Du, M. H.; Singh, D. J.; Podlesnyak, A.; Ehlers, G.; Lumsden, M. D.; Sales, B. C. *Nature Materials* **2011**, *10*, 614.

(28) Ahmad, S.; Mahanti, S. D.; Hoang, K.; Kanatzidis, M. G. *Phys. Rev. B* **2006**, *74*, 155205.

(29) Xiong, K.; Lee, G.; Gupta, R. P.; Wang, W.; Gnade, B. E.; Cho, K. *J. Phys. D: Appl. Phys.* **2010**, *43*, 405403.

(30) Ahmad, S.; Hoang, K.; Mahanti, S. D. *Phys. Rev. L* **2006**, *96*, 056403.

(31) Singh, D. J. *Phys. Rev. B* **2010**, *81*, 195217.

(32) Airapetyants, S. V.; Vinogradova, M. N.; Dubrovskaya, I. N.; Kolomoets, N. V.; Rudnik, I. M. *Soviet Physics-Solid State* **1966**, *8*, 1069.

(33) Khokhlov, D. *Lead Chalcogenides Physics and Applications*; Taylor & Francis Books; New York & London, 2003.

(34) Allgaier, R. S. *J. Appl. Phys.* **1961**, *32*, 2185.

(35) Parker, D.; Singh, D. J. *Phys. Rev. B* **2010**, *82*, 035204.

(36) Noda, Y.; Orihashi, M.; Nishida, I. A. *Mater. Trans., JIM* **1998**, *39*, 602.

(37) Ravich, Y. I.; Efimova, B. A.; Smirnov, I. A. *Semiconducting Lead Chalcogenides*; Plenum, 1970.

(38) Crocker, A. J.; Rogers, L. M. *Brit J Appl Phys* **1967**, *18*, 563.

(39) Svane, A.; Christensen, N. E.; Cardona, M.; Chantis, A. N.; van Schilfgaarde, M.; Kotani, T. *Phys. Rev. B* **2010**, *81*, 245120.

(40) It should be noted that the gap between conduction and heavy hole bands in PbTe is typically taken to be $\Delta E_{C-\Sigma} = 0.36$ eV. As shown in the Supporting Information, we found a poorer fit to the data using this value of $\Delta E_{C-\Sigma}$ compared to the value of $\Delta E_{C-\Sigma} = 0.42\,\mathrm{eV}$ given in Eq. 9.

(41) Jaworski, C. M.; Wiendlocha, B.; Jovovic, V.; Heremans, J. P. *Energy Environ. Sci.* **2011**, *4*, 4155.

(42) Pei, Y. Z.; LaLonde, A. D.; Heinz, N. A.; Shi, X. Y.; Lwanaga, S.; Wang, H.; Chen, L. D.; Snyder, G. J. *Adv. Mater.* **2011**, *23*, 5674.

(43) Biswas, K.; He, J. Q.; Zhang, Q. C.; Wang, G. Y.; Uher, C.; Dravid, V. P.; Kanatzidis, M. G. *Nature Chemistry* **2011**, *3*, 160.

(44) Zhang, Q. Y.; Wang, H. Z.; Zhang, Q.; Liu, W. S.; Yu, B; Wang, H.; Wang, D. Z.; Ni, G.; Chen, G.; Ren, Z. F. *Nano Lett.* **2012**, DOI: 10.1021/nl3002183.

(45) Jaworski, C. M.; Heremans, J. P. *Phys. Rev. B* **2012**, *85*, 033204.

(46) Volkov, B. A.; Ryabova, L. I.; Khokhlov, D. R. *Phys. Usp.* **2002**, *45*, 819.

(47) Jovovic, V.; Thiagarajan, S. J.; Heremans, J. P.; Komissarova, T.; Khokhlov, D.; Nicorici, A. *J. Appl. Phys.* **2008**, *103*, 053710.

(48) Pei, Y. Z.; Lensch-Falk, J.; Toberer, E. S.; Medlin, D. L.; Snyder, G. J. *Adv. Funct. Mater.* **2011**, *21*,241.

TOC:

Pisarenko relations were plotted in potassium (K) doped $PbTe_{1-y}Se_y$ samples where one could find that the use of Se effectively increases the carrier concentration and heavy doping was achieved by activation of the heavy hole band. Maximum peak *ZT* appears in Se-rich $K_{0.02}Pb_{0.98}Te_{0.15}Se_{0.85}$, but the average *ZT*s are higher in Te-rich sample $K_{0.02}Pb_{0.98}Te_{0.75}Se_{0.25}$ than the Se-rich samples $K_{0.02}Pb_{0.98}Te_{0.15}Se_{0.85}$.

Qian Zhang, Feng Cao, Weishu Liu, Kevin Lukas, Bo Yu, Shuo Chen, Cyril Opeil, David Broido, Gang Chen and Zhifeng Ren

Heavy doping and band engineering by potassium to improve thermoelectric figure-of-merit in p-type PbTe, PbSe, and $PbTe_{1-y}Se_y$

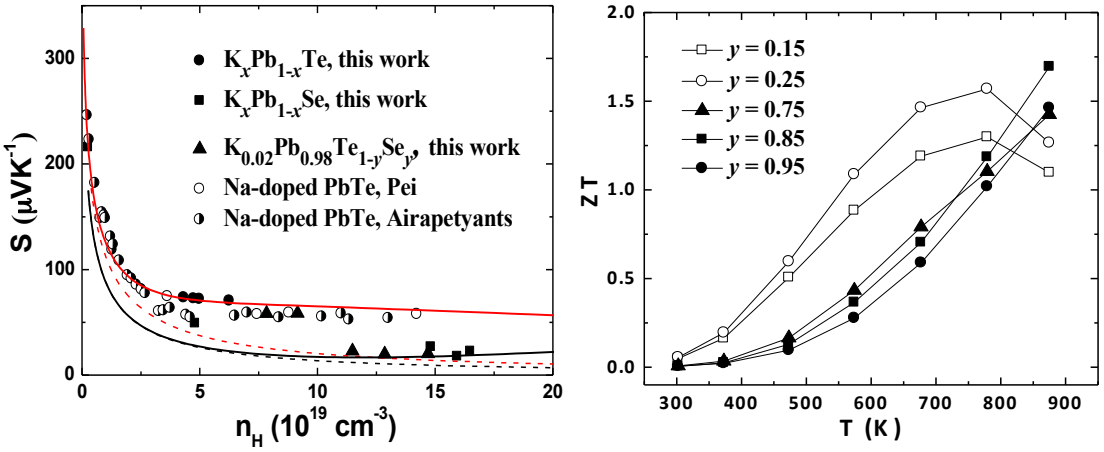

Supporting information

Heavy doping and band engineering by potassium to improve thermoelectric figure-of-merit in p-type PbTe, PbSe, and $PbTe_{1-y}Se_y$

Qian Zhang,[†] Feng Cao,[†] Weishu Liu,[†] Kevin Lukas,[†] Bo Yu,[†] Shuo Chen,[†] Cyril Opeil,[†] David Broido,[†] Gang Chen,*[‡] and Zhifeng Ren**[†]

[†] Department of Physics, Boston College, Chestnut Hill, Massachusetts 02467, USA

[‡] Department of Mechanical Engineering, Massachusetts Institute of Technology, Cambridge, Massachusetts 02139, USA

Corresponding Author

*gchen2@mit.edu

**renzh@bc.edu

The microstructures were investigated by a scanning electron microscope (SEM, JEOL 6340F) and a high resolution transmission electron microscope (HRTEM, JEOL 2010F). The chemical composition was analyzed on an energy-dispersive X-ray (EDX) spectrometer attached to SEM.

Table S1. Comparison between nominal composition and real composition (detected by EDS) for some samples.

Nominal composition	$K_{0.015}Pb_{0.985}Te$	$K_{0.0125}Pb_{0.9875}Se$	$K_{0.02}Pb_{0.98}Te_{0.15}Se_{0.85}$	$K_{0.02}Pb_{0.98}Te_{0.75}Se_{0.25}$
Real composition	$K_{0.014}Pb_{0.944}Te_{1.042}$	$K_{0.013}Pb_{0.967}Se_{1.02}$	$K_{0.02}Pb_{0.976}Te_{0.162}Se_{0.842}$	$K_{0.019}Pb_{0.967}Te_{0.733}Se_{0.281}$

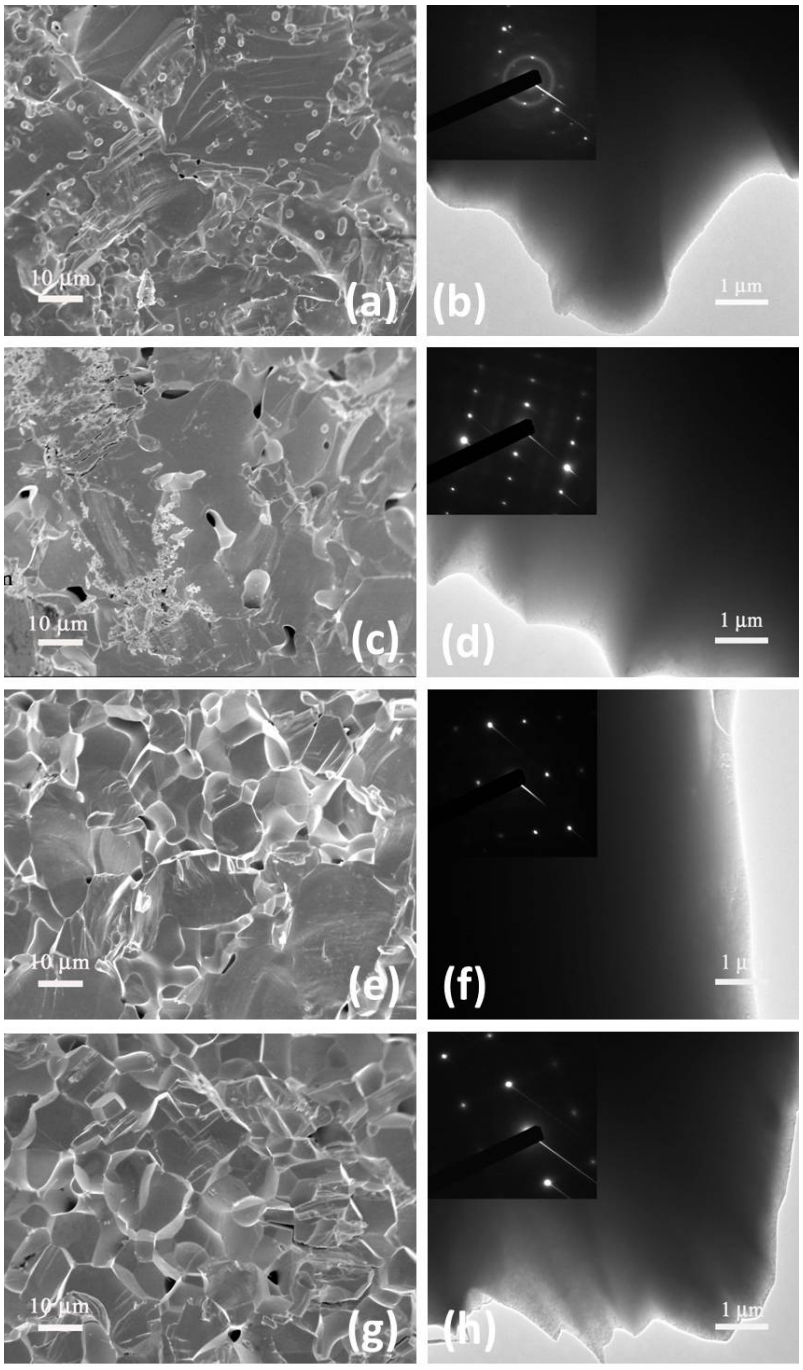

Figure S1. SEM images of samples $K_{0.015}Pb_{0.985}Te$ (a), $K_{0.02}Pb_{0.98}Te_{0.75}Se_{0.25}$ (c), $K_{0.02}Pb_{0.98}Te_{0.15}Se_{0.85}$ (e) and $K_{0.0125}P_{b0.9875}Se$ (g), respectively. TEM images of samples $K_{0.015}Pb_{0.985}Te$ (b), $K_{0.02}Pb_{0.98}Te_{0.75}Se_{0.25}$ (d), $K_{0.02}Pb_{0.98}Te_{0.15}Se_{0.85}$ (f) and $K_{0.0125}P_{b0.9875}Se$ (h), respectively. The insets in (b), (d), (f) and (h) are the selected area electron diffraction (SAED) patterns.

For Reference 40

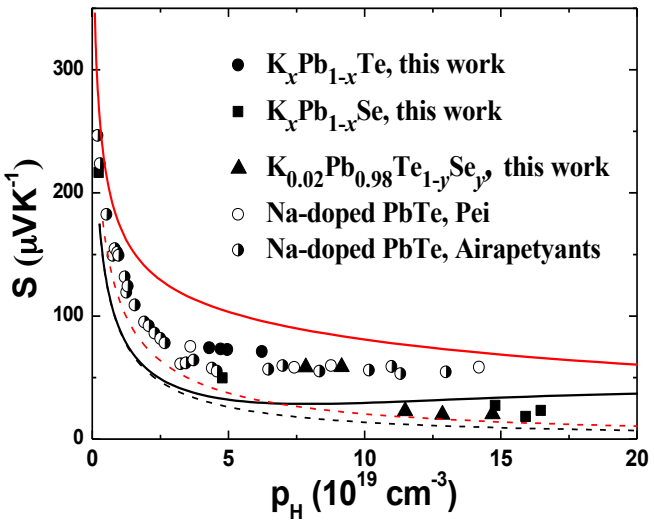

Figure S2. Room temperature Pisarenko plots for $K_xPb_{1-x}Te$ (x = 0.01, 0.0125, 0.015, and 0.02, filled circles), $K_xPb_{1-x}Se$ (x = 0, 0.005, 0.010, 0.0125, and 0.015, filled squares), and $K_{0.02}Pb_{0.98}Te_{1-y}Se_y$ (y = 0.15, 0.25, 0.75, 0.85, and 0.95, filled triangles) in comparison with reported data on Na-doped PbTe by Pei *et al.*[20] (open circles) and Airapetyants *et al*[32] (half open circles). Dashed black curve is based on single nonparabolic band model with the light hole effective mass of PbSe m^*/m_e = 0.28. Solid black curve is based on two bands model (light nonparabolic band and heavy parabolic band) with the heavy hole effective mass of PbSe m^*/m_e = 2.5. Dashed red curve is based on single nonparabolic band model with the light hole effective mass of PbTe m^*/m_e = 0.36. Solid red curve is based on two bands model (light nonparabolic band and heavy parabolic band) with the heavy hole effective mass of PbTe m^*/m_e = 2.

We calculate the relationship between carrier concentrations of light hole and heavy hole bands, p_L, and p_Σ, and the Hall carrier concentration p_H using function below,[25,37]

$$p_H = [bp_L + p_\Sigma]^2 / [A_L b^2 p_L + A_\Sigma p_\Sigma] \quad (1)$$

where A_L is Hall factor for L band, and A_Σ is the Hall factor for the Σ band. Expressions for A_L and A_Σ have been presented previously[37]. The parameter, b is the mobility ratio of L band to Σ band, which depends weakly on temperature. Here we take $b = 4$ as found in Ref. 25. For the single band model, $p_H = p_L / A_L$. Figure S3 below shows difference between p_H and the total carrier concentration, $p = p_L + p_\Sigma$.

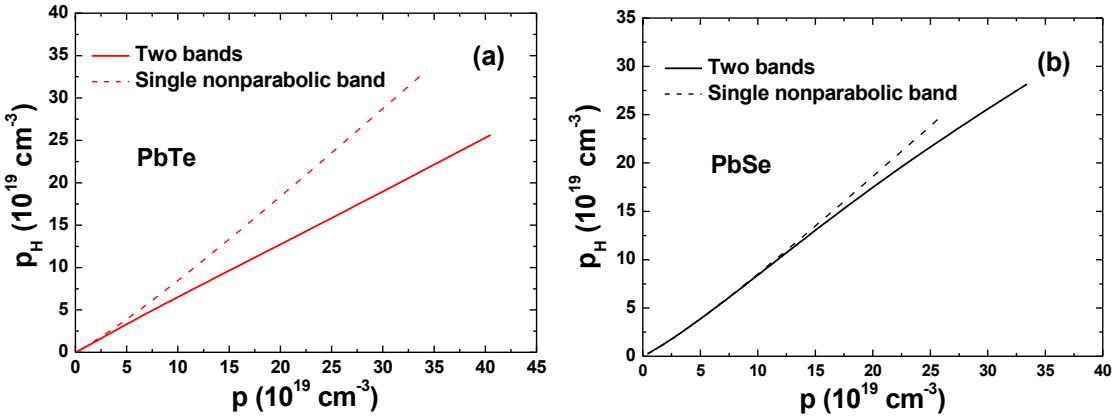

Figure S3. The relationship between carrier concentration and Hall carrier concentration for PbTe (a) and PbSe (b).